Friction **10**(6): 944–962 (2022)
https://doi.org/10.1007/s40544-021-0544-y
ISSN 2223-7690
CN 10-1237/TH
RESEARCH ARTICLE

A finite-element-aided ultrasonic method for measuring central oil-film thickness in a roller-raceway tribo-pair

Pan DOU[1], Tonghai WU[1,*], Zhaopeng LUO[1], Peiping YANG[2], Zhongxiao PENG[3], Min YU[4], Tom REDDYHOFF[4]

[1] *Key Laboratory of Education Ministry for Modern Design and Rotor-Bearing System, Xi'an Jiaotong University, Xi'an 710049, China*

[2] *Dongfang Electric Machinery Co., Ltd., Deyang 618000, China*

[3] *School of Mechanical and Manufacturing Engineering, University of New South Wales, Sydney 2052, Australia*

[4] *Department of Mechanical Engineering, Imperial College London, London SW7 2AZ, UK*

Received: 08 January 2021 / Revised: 06 April 2021 / Accepted: 21 July 2021

Abstract: Roller bearings support heavy loads by riding on an ultra-thin oil film (between the roller and raceway), the thickness of which is critical as it reflects the lubrication performance. Ultrasonic interfacial reflection, which facilitates the non-destructive measurement of oil-film thickness, has been widely studied. However, insufficient spatial resolution around the rolling line contact zone remains a barrier despite the use of miniature piezoelectric transducers. In this study, a finite-element-aided method is utilized to simulate wave propagation through a three-layered structure of roller-oil-raceway under elastohydrodynamic lubrication (EHL) with nonlinear characteristics of the i) deformed curvature of the cylindrical roller and ii) nonuniform distribution of the fluid bulk modulus along the circumference of the oil layer being considered. A load and speed-dependent look-up table is then developed to establish an accurate relationship between the overall reflection coefficient (directly measured by an embedded ultrasonic transducer) and objective variable of the central oil-film thickness. The proposed finite-element-aided method is verified experimentally in a roller-raceway test rig with the ultrasonically measured oil-film thickness corresponding to the values calculated using the EHL theory.

Keywords: ultrasonic measurement; central oil-film thickness; rolling line contact; ray model; finite-element-aided method

1 Introduction

The Rolling bearings are critical supporting components of rotating machinery. An ultra-thin film of oil, which exists between the roller and raceway and typically forms based on dynamic lubrication effects, can support heavy loads. This thin oil film has an important role in bearing operations by reducing friction and wear, extending their lifespan, and/or dissipating heat [1].

The elastohydrodynamic lubrication (EHL) theory (e.g., Dowson's theory) is widely used to predict oil-film thickness in a finite line contact and frequently requires the support of measured data for validation, especially in industrial applications [2–4]. The accurate measurement of oil film thickness provides not only fundamental and valuable information on the lubrication status for early warning of lubrication failures, but also the measured data for verification of the EHL theory. However, the accurate acquisition of the oil-film thickness under operating conditions remains an ongoing challenge for line-contact components such as roller bearings owing to the limited space for the installation of a transducer and the required measurement spatial resolution of the thin oil film at a micrometer or submicron scale.

Among conventional methods [5–11], the ultrasonic-

* Corresponding author: Tonghai WU, E-mail: wt-h@163.com

based method [11] has been widely studied owing to its non-destructive nature. To date, a group of ultrasonic-based measurement models have been developed to calculate the film thickness variation in different lubrication regimes [11–15]. Among these models, the spring model [11] is deemed to be particularly suitable for thin-film thicknesses, e.g., less than 10 μm. However, the spring model is only valid under the assumption that the tribo-pairs are composed of two parallel and rigid surfaces. Conversely, roller bearings have nonparallel and curved surfaces; the thickness and stiffness of the oil film between the two surfaces are nonuniformly distributed owing to the varied stresses in the contact, significantly influencing the ultrasonic measurements; moreover, the width of the line-contact zone is typically small compared to that of the transducer. Given these complexities, improving the spatial resolution is frequently the focus of this promising technique. Attempts have been made to improve the resolution of the hardware of ultrasonic transducers. The focusing lens and liquid bath were used to focus the acoustic beam, thus improving the spatial resolution [16]. The higher the center frequency of the transducer, the smaller the focal zone of the focusing transducer [17]. However, high frequencies induce increasing attenuation in the sound energy, making the influence of the thickness of the steel ring non-negligible when practicing this method. Moreover, an additional hole is required on the bearing housing to fix the transducer, acoustic lens, and cables.

Progress was reported by Drinkwater et al. [18] in 2009. In their study, a piezoelectric thin-film ultrasonic transducer of 200 MHz was attached to the outer raceway of a deep groove ball bearing to monitor the oil film. The active area of this transducer was approximately 0.3 mm in width and 3 mm in length, and its focus area was less than that of the contact area. However, piezoelectric thin-film ultrasonic transducers are expensive and complex. Moreover, as described above, high-frequency ultrasonic waves tend to be significantly attenuated during propagation, making the captured data sensitive to signal noise. Other researchers have focused on using low-cost piezoelectric elements that are cut into smaller rectangular pieces to improve the spatial resolution [19, 20]. This is not a feasible solution for industrial applications owing to the difficulty of maintaining these brittle and tiny transducers. Furthermore, such a simple cut divides the energy of the ultrasonic signal and thus decreases the signal-to-noise ratio. To date, the narrowest rectangular piezoelectric element is 0.6 mm [20].

Other researchers have developed new signal processing algorithms to extract the exact film thickness; however, at the cost of the repetition frequency of the measurement [21, 22]. When measuring using a focusing transducer, under low speed and high-repetition frequency, the focal spot moves sufficiently slowly such that the two adjacent focused spot circles overlap in the diameter when the rollers pass by the fixed transducer. By analyzing the internal relationship between the multiple overlapped measuring points, the reflection coefficient of the overlapped region of consecutive measuring points can be obtained. The overlapped area of two consecutive measuring points is smaller than that of the focal zone, and thus a higher resolution can be obtained. However, as the bearing speed increases, the overlapped region of the two consecutive measuring points decreases or even disappears.

Using a rectangular piezoelectric element, a ray model was proposed for practical applications in ultrasonic measurements. This equates the sonic field to a cluster of rays. Each ray can be used to calculate the oil-film thickness based on the hypothesis of total reflection. For nonparallel surfaces, the surface profile is considered to extract the reflection coefficient of the central film thickness from the overall reflection coefficient using the ray model. This practice was performed in a piston ring and cylindrical roller bearing [19, 20]. The results demonstrated that the ray model can improve the measurement resolution to a certain degree. However, the ray model ignores the scatter influence caused by the curved surface profile and influence of the nonuniform distribution of the bulk modulus in the oil layer. A detailed analysis with the ray model is presented in Section 2.2, with its limitations to the thickness measurement of oil film between nonparallel interfaces indicated.

This study adopts a finite-element-aided method to simulate wave propagation through a three-layered

structure of roller-oil-raceway under EHL with nonlinear characteristics of the i) deformed curvature of the cylindrical roller and ii) nonuniform distribution of the fluid bulk modulus along the circumference of the oil layer being considered. A load- and speed-dependent look-up table is then developed to establish an accurate relationship between the overall reflection coefficient (directly measured by an embedded ultrasonic transducer) and objective variable of the central oil-film thickness.

The remainder of this paper is organized as follows: Section 2 reviews the ultrasonic spring model and analyses the limitations of the ray model, which is commonly employed to calculate the oil-film thickness in a roller bearing. Section 3 proposes an finite element method (FEM) to aid film thickness measurement, and the effectiveness of this method is demonstrated by comparing the simulated reflection coefficient with the theoretical reflection coefficient in a simplified three-layered parallel lubrication model. With the proven feasibility, Section 4 uses the FEM again for *in situ* oil-film thickness measurement in a roller-raceway contact under EHL, where a mathematical relationship between the measurable ultrasonic reflection coefficient and central film thickness is established to ensure accurate measurements. Section 5 presents the test setup and discusses the experimental testing results to assess the proposed FEM-aided method. Finally, conclusions are presented in Section 6.

2 Ultrasonic-based measurement in roller-raceway contact

This section introduces the principle of the classical spring model, based on which a commonly used ray model is introduced to measure the oil-film thickness in a roller bearing. The limitations of the ray model, particularly in terms of measurement resolution, are further analyzed.

2.1 Principle of spring model

In a three-layered structure of steel–oil–steel with all surfaces parallel, ultrasonic waves that perpendicularly incident on the oil layer would be transmitted and reflected partially at each interface simultaneously. Assuming that the oil layer is between two surfaces with the same steel material, the reflection coefficient from the oil layer can be expressed as [23]

$$\left|R(f)\right| = \sqrt{\frac{\left(\frac{z}{z_0}-\frac{z_0}{z}\right)^2 \sin^2\left(\frac{2\pi hf}{c}\right)}{4+\left(\frac{z}{z_0}-\frac{z_0}{z}\right)^2 \sin^2\left(\frac{2\pi hf}{c}\right)}} \tag{1}$$

where $\left|R(f)\right|$ is the reflection coefficient, h is the thickness of the oil-film layer, f is the frequency of the incident signal, and z_0 and z are the acoustic impedances of the oil film and steel, respectively. The impedance of oil z_0 is calculated using $z_0 = \rho c$, where ρ is the density of the oil and c is the wave speed of the oil.

When the oil layer thickness is thinner than the ultrasonic wavelength, the elastic effect of the oil layer becomes dominant in the load support. In this case, Eq. (1) can be simplified to a quasistatic spring model [24]:

$$h = \frac{B}{\pi f z}\sqrt{\frac{\left|R(f)\right|^2}{1-\left|R(f)\right|^2}} \tag{2}$$

where B is the bulk modulus of the fluid, expressed as

$$B = \rho c^2 \tag{3}$$

As the incident signal is difficult to obtain, the reflection coefficient is normally obtained by comparing the signal reflected from the oil layer to that from a reference interface with known acoustic impedance [12]:

$$\left|R(f)\right| = \frac{A_{\mathrm{mf}}}{A_{\mathrm{ref}}}\left|R_{\mathrm{ref}}(f)\right| \tag{4}$$

where $A_{\mathrm{mf}}(f)$ is the amplitude of the reflected signal from the solid/oil interface, the amplitude of the reference signal is denoted as $A_{\mathrm{ref}}(f)$, and the reflection coefficient of the reference interface is denoted by $\left|R_{\mathrm{ref}}(f)\right|$. In the case of full reflection (i.e., no wave penetration), $\left|R_{\mathrm{ref}}(f)\right|$ is equal to 1.

2.2 Ray model for measuring oil film in roller-raceway contact

The principle of the ultrasonic-based oil-film thickness

measurement in a roller-raceway tribo-pair is depicted in Fig. 1. An ultrasonic transducer is used to emit ultrasonic waves and collect the reflected signals from the oil film. With these waves, the thickness can be calculated with the spring model using Eqs. (2) and (4).

As can be observed in Fig. 1, the roller-raceway contact zone is composed of the central flat contact and two curvature segments considering the lubrication film. The sonic wave reflection could fully cover the contact zone if the transducer is wider than the flat contact zone. This is commonly observed in practice because the contact width is on the micron scale, whereas the transducer is on the millimeter scale. Therefore, the average value of the oil-film thickness must be compromised in practical measurements, instead of a more meaningful value of the central oil-film thickness in a lubricated contact.

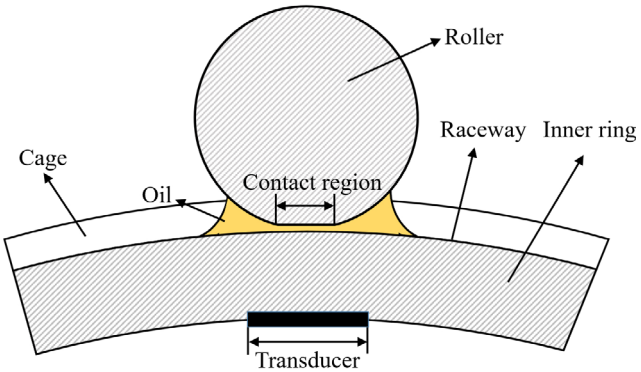

Fig. 1 Schematic diagram of the ultrasonic measurement of oil-film thickness in roller-raceway tribo-pair.

To describe the central thickness in a real contact zone, the ray model is proposed [19, 20]. The principle is to divide the sonic field into small equal units along the transducer width (Fig. 2(a)). In each unit, the ultrasound wave propagates vertically and independently. Considering the complicated oil-film shape within the transducer width, three parts of the acoustic field are identified: the central part (denoted as v) and two wedge parts on the left, and right ends (denoted as u and w, respectively).

The oil-film thickness in each part corresponds to an individual reflection coefficient. Therefore, the reflection coefficient is the average of the values within the entire width of the transducer.

$$R_{\text{ray}} = \sum_{i=0}^{n} \frac{R(h_i)\Delta x}{l} \tag{5}$$

where R_{ray} is the overall reflection coefficient over the entire width (l) of the piezoelectric element, $R(h_i)$ is the individual reflection coefficient of the i-th wave component, with an effective width of Δx and the corresponding film thickness h_i, and n is the total number of wave components.

The ray model is initially used to correct the measured reflection coefficient, with the geometric deformation in the contact area of the roller-raceway accommodated [18]. Subsequently, it is used to extract the central oil-film thickness from the overall reflection coefficient, provided that the surface profile can be theoretically given [19, 20].

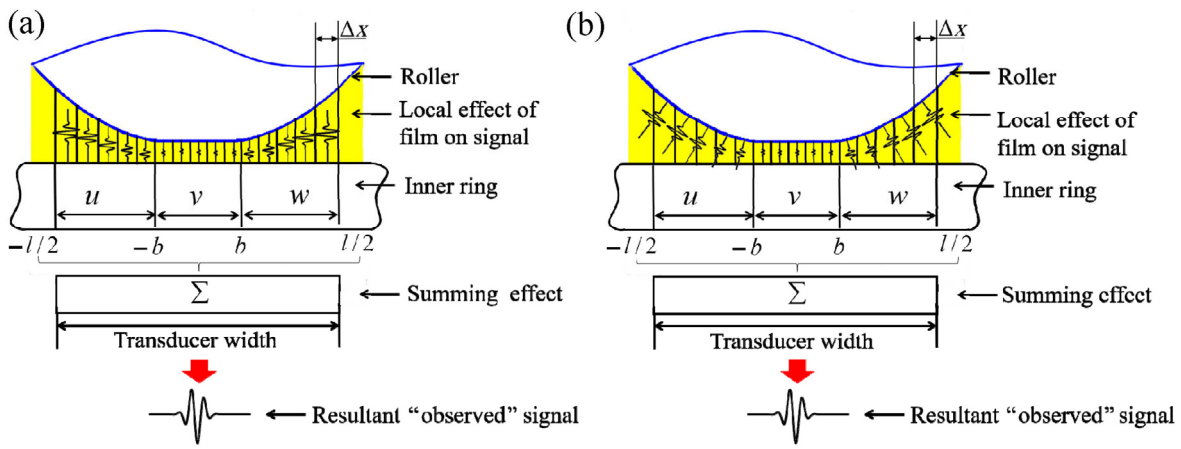

Fig. 2 Schematic diagrams of ray model principle: (a) Rays are perpendicular to raceway surface and (b) rays are perpendicular to roller surface. l is the width of the transducer. b is the half-width of the contact zone.

In application, using the measured and calculated average oil-film thicknesses, an iterative matching method is adopted to extract the central film thickness. The central film thickness is added gradually with a definite interval from zero. The average reflection coefficient, R_{ray}, for each central film thickness is calculated using Eq. (5). This iteration is terminated when the discrepancy between the measured and calculated values of the average oil-film thickness is within the preset error. Consequently, the final central film thickness can be extracted from the calculation of the ray model.

Fundamentally, a complete vertical reflection of sonic waves is assumed in the ray model, irrespective of the convex surfaces by which the echoes are received by the transducer [19, 20]. This is far from the reality where scattering occurs on nonparallel surfaces including convex surfaces. Therefore, an alternative illustration is depicted in Fig. 2(b), where the reflected waves from the nonparallel interfaces (u and w, the two side parts) are no longer in the vertical direction. Different reflections correspond to the different parts of the lubrication zone. Consequently, large errors are inherent with the vertical reflection assumption, especially under non-ignored contact deformation [25].

Another problem is that the bulk modulus of the oil layer is assumed to be uniform in the contact zone in the traditional ray model [20]. Based on classical EHL theory, the metal surfaces in the high-stress contact zone are elastically deformed, and the bulk modulus of the oil film cannot be simply taken as a constant value owing to the nonuniformly distributed oil stress. It can be inferred from Eq. (2) that the variation in the bulk modulus would change the reflection coefficient. However, the influence of the ray model on the calculation error has not been considered in existing studies [18–20]. Given this issue, the measurement errors caused by the ray model are comprehensively investigated and further quantified using a finite element simulation method in this study, leading to highly accurate calculation results of the central oil-film thickness in a roller-raceway contact.

3 FEM-based acoustic simulation of parallel three-layered structure

The FEM has been widely adopted in simulating ultrasonic propagation [26–28]; however, it has not yet been suggested for measuring oil-film thickness. In this section, a simplified parallel three-layered model was used to demonstrate the effectiveness of the proposed FEM approach for the theoretical calculation of oil-film thickness.

The commercial software COMSOL Multiphysics (version 5.3) [26, 27] was used for the FEM simulations. Two modules, the linear elastic module for steel deformation and acoustic pressure module with a line acoustics source were included. By inputting an exciting signal into the acoustic source, the normal incidence of ultrasonic waves can be modeled and thereby, the sonic field in all media can be obtained [28]. The simulation included seven steps, summarized as follows.

1) Build the three-layered geometric model (steel–oil–steel parallel structure);

2) Set the material property parameters (elasticity modulus, density, and Poisson's ratio for the steel and sound speed, and density for the oil) of all media;

3) Assign the linear elastic material and acoustic pressure modulus to the steel and oil medium, respectively;

4) Input the disturbance signal to the line source and adopt the time-dependent study modulus to compute the time-varying propagation of the pressure waves;

5) Discretize the model with varying meshes;

6) Set the time-dependent solver;

7) Solve and derive the result.

To avoid distortion of the waveform in the propagation, the maximum mesh size is suggested to be less than 1/5 of the wavelength [27, 28]. In this study, the wavelength is defined as the ratio of the speed of sound to the wave frequency. Therefore, the maximum frequency of the simulated ultrasonic wave determines the size of the largest element size. In addition, a free subdivision triangular mesh was adopted considering its advantage of adaptive refinement [26–28]. Although the calculation cost increases with a decrease in the mesh size, the selection of the mesh size in this study is mainly concerned with a high measurement accuracy rather than computational efficiency.

Overall, the mesh is adaptively controlled by five parameters: maximum element size, minimum element size, maximum element growth rate, curvature factor,

and resolution of the narrow regions. The maximum element size is used to limit the allowable element size. The resolution of the narrow regions is used to control the number of element layers in the thin oil-film regions.

The model and meshing results of the parallel three-layered (steel–oil–steel) structure are displayed in Fig. 3. Rather than a transducer with a width of 7 mm as used in our previous works [12, 13, 15], a considerably smaller transducer with 0.6 mm width was utilized in this study to further improve the spatial resolution of the measurement. The maximum element sizes inside and outside the transducer diameter were 0.09 mm (namely 1/10 of the minimum wavelength) and 0.3 mm, respectively. The minimum element size, maximum element growth rate, curvature factor, and resolution of the narrow regions were 0.00001 mm, 1.3, 0.3, and 1, respectively.

A Gaussian wave was used as the incident ultrasonic wave [29] taking the following form:

$$f(t) = A\mathrm{e}^{-\left(f_0(t-3T_0)^2\right)}\sin\left(2\pi f_0 t\right) \tag{6}$$

where A ($A = 1\times10^{-8}$ mm) is the amplitude of the Gaussian wave, f_0 ($f_0 = 12.5$ MHz) is the center frequency of the Gaussian wave, and $T_0 = 1/f_0$.

The reference wave was obtained by replacing the oil with air. The reflection coefficient, namely the simulated reflection coefficient, was calculated using Eq. (4). For comparison, several film thicknesses of 1, 2, 3, and 4 μm were simulated with different calculation time of 7 h 42 m 51 s, 4 h 21 m 27 s, 2 h 20 m 23 s, and 1 h 31 m 55 s, respectively.

To validate the FEM simulation, the theoretical reflection coefficients were also calculated using Eq. (1) with the same oil-film thickness. These two reflection coefficients are plotted together in Fig. 4 with their deviations from each other.

Acceptable consistency between the theoretical and simulation results can be drawn from Fig. 4, where the overall relative error ranges from −0.06% to +0.06% in the testing frequency bandwidth of 10.3–16.6 MHz (−6 dB). However, significant errors can be identified at both ends of the frequency band, including zones less than 3 MHz and greater than 23 MHz. Such large errors can be analyzed by inspecting the solving criterion of the FEM. Iterations with relative termination tolerance were primarily adopted in the FEM software. However, the wave amplitude near the limits of the effective frequency bandwidth attenuated significantly. When the wave amplitude was small and close to the relative tolerance, the number of iterations was limited. Therefore, the effective frequency bandwidth should be considered in further analyses.

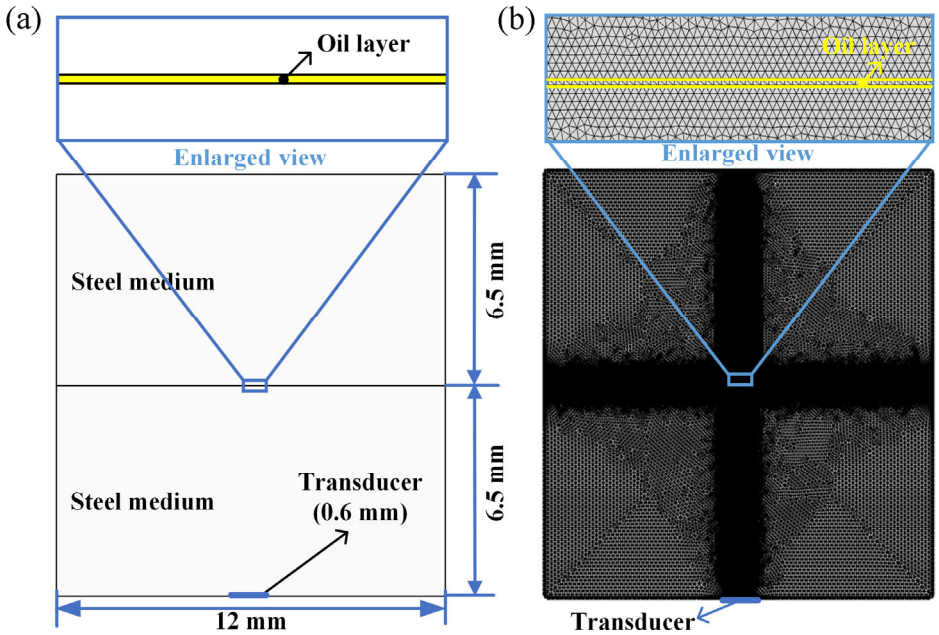

Fig. 3 (a) FEM of parallel steel–oil–steel structure and (b) corresponding meshing result.

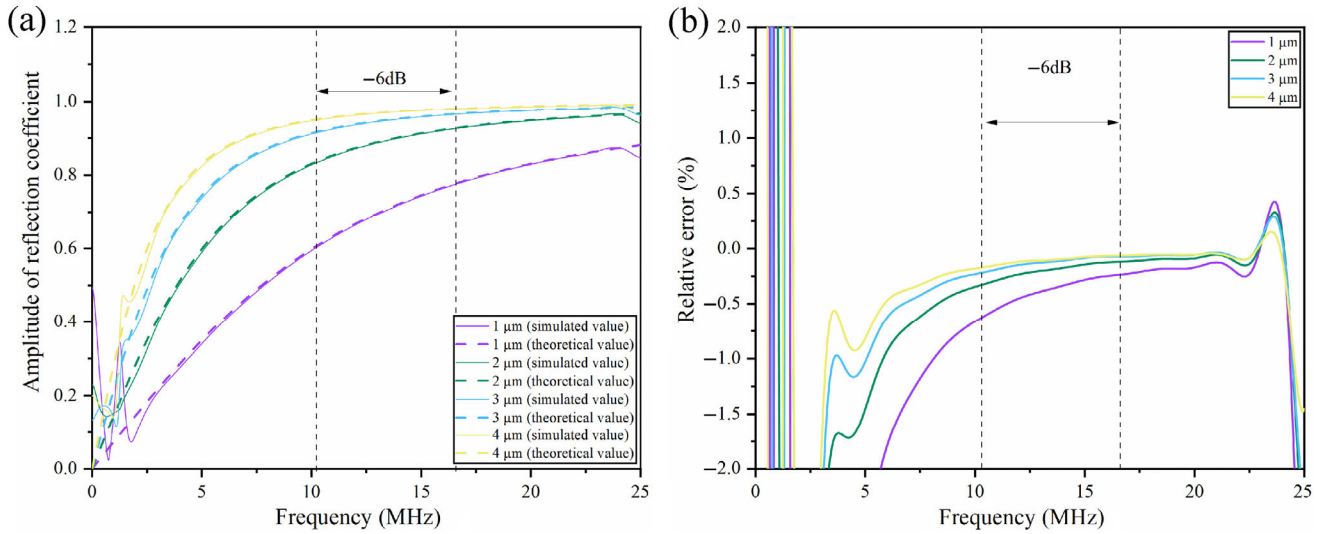

Fig. 4 Simulated and theoretical reflection coefficients, and relative errors at four different oil-film thicknesses: (a) reflection coefficient and (b) relative error.

4 FEM-based calculation of oil-film thickness in roller-raceway contact

With the proof of the FEM-aided oil-film thickness measurement stated above, in this section, acoustic simulations with a roller-raceway contact are conducted under different operating conditions (Section 4.1) to obtain accurate oil-film thicknesses. The error of the ray model is quantified by comparing it with the simulation results (Section 4.2), addressing the two error sources. With the simulation to verify the error source of the ray model, the acoustic simulation is used to separately analyze the influence of the geometric scattering at the lubrication interface and the nonuniform distribution of the bulk modulus of the oil layer on the ray model (Section 4.3). An FEM-aided method is proposed to extract the central oil-film thickness by considering the load and speed compensation (Section 4.4).

4.1 Acoustic FEM simulations for an equivalent roller-raceway model

The contact of a roller-raceway under lubrication is complicated because it involves both solid deformation and uneven loading of the oil film. According to the line contact EHL theory proposed by Wen and Huang [2] and Grubin [3], the shape of the lubricant film formed by the contact of two elastic cylinders can be equivalent to the shape of the lubricant film formed by the contact of an equivalent cylinder with a rigid plane. Therefore, such an equivalence principle is adopted to depict the roller-raceway contact under identical conditions.

According to the EHL theory, the oil-film thickness in the contact zone (h_v) and surrounding gap zone (h_g) can be obtained from Eqs. (7) and (8), respectively [2]:

$$\frac{h_v}{R'} = 1.95\left(\frac{U\eta_0\alpha}{R'}\right)^{\frac{8}{11}}\left(\frac{E'LR'}{W}\right)^{1/11}, |x| \le b \tag{7}$$

$$h_g = \frac{2bp_0}{E'}\left[\frac{x}{b}\sqrt{\frac{x^2}{b^2}-1} - \ln\left(\frac{x}{b}+\sqrt{\frac{x^2}{b^2}-1}\right)\right], |x| < b \tag{8}$$

where U is the entrainment speed, η_0 is the lubricant viscosity at the contact entry, α is the pressure–viscosity coefficient, E' is the reduced elastic modulus of the roller material, W is the load on the contact, b is the half-width of the contact zone, x is the distance from the origin to the position to be solved, and p_0 is the maximum contact stress in the contact zone. It can be expressed as

$$b = \left(\frac{8WR'}{\pi LE'}\right)^{1/2} \tag{9}$$

where L is the roller length.

$$p_0 = \left(\frac{E'b}{4R'}\right)^{1/2} \tag{10}$$

where R' is the reduced radius of curvature, given by

$$\frac{1}{E'}=\frac{1}{2}\left(\frac{1-\upsilon_1^2}{E_1}+\frac{1-\upsilon_2^2}{E_2}\right) \tag{11}$$

$$\frac{1}{R'}=\frac{1}{R_1}+\frac{1}{R_2} \tag{12}$$

where E is Young's modulus and υ is Poisson's ratio. Subscripts 1 and 2 refer to the roller and raceway, respectively. The parameters required to calculate the theoretical oil-film shapes are listed in Table 1.

Table 1 Parameters in EHL film thickness calculations [20].

Parameter	Value
Reduced modulus, E' (GPa)	214.5
Reduced radius, R' (mm)	54
Pressure viscosity coefficient for T68, α (GPa^{-1})	22
Effective viscosity for T68, η_0 ((N·m)/m^2)	0.2
Length of the roller, L (mm)	10

The two-dimensional model of the roller-oil-raceway based on Hertz theory is displayed in Fig. 5. The half-width of the contact zone, b, can be calculated using Eq. (9).

The pressure distribution in the contact zone conforms to a half-elliptical distribution [2].

$$p=p_0\left(1-\frac{x^2}{b^2}\right) \tag{13}$$

The bulk modulus of the oil layer, as influenced by the high contact stress, is given by [30, 31]

$$B=\left\{1-\frac{1}{1+B_0'}\log_e\left[1+\frac{p_1}{B_0}\left(1+B_0'\right)\right]\right\}\left[B_0+p_1\left(1+B_0'\right)\right] \tag{14}$$

where p_1 is the pressure in the liquid, B_0 is the bulk modulus at ambient pressure, and B_0' is the pressure rate of change of B at ambient pressure, which is approximately 11 [31]. B_0 can be calculated using Eq. (15) [32, 33]:

$$B_0=B_{00}\exp\left(-\beta_k T\right) \tag{15}$$

where B_{00} and β_k are the constant coefficients. B_{00} is approximately 12 GPa, β_k is approximately 6.5e10^{-3} K^{-1}, and T is the absolute temperature. The density of the oil layer under pressure p, ρ_p, is given by Eq. (16) [2]:

$$\rho_p=\rho_0\left(1+\frac{0.6p}{1+1.7p}\right) \tag{16}$$

where p is the speed of sound under pressure and ρ_0 is the density of the oil layer under pressure p_0.

Figure 6 displays the distribution of the bulk modulus within the transducer width under different loads. It can be observed that the distribution of the bulk modulus is uniform and largely ranges along the contact width. Distribution uniformity is defined numerically as the difference between the maximum and minimum values throughout the contact width, which is proportional to the load.

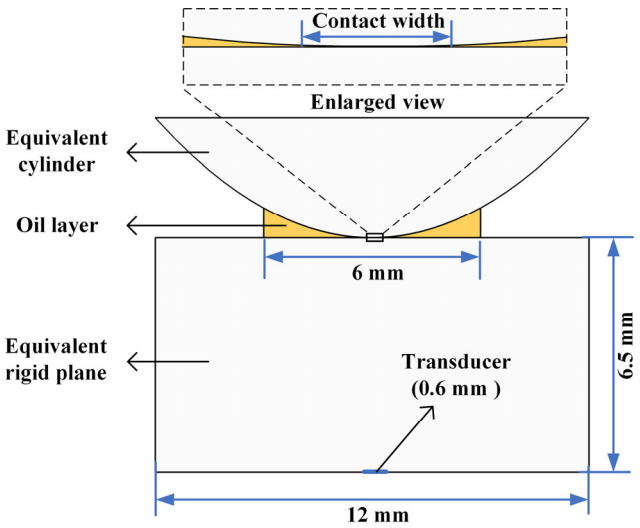

Fig. 5 Equivalent model of roller-raceway contact.

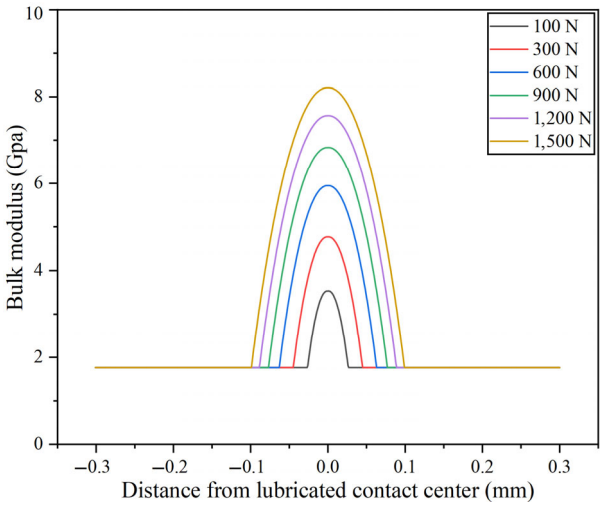

Fig. 6 Distribution of oil bulk modulus in roller-raceway contact with load varied from 100 to 1,500 N.

The p can be obtained by combining Eqs. (2) and (14)–(16). The center frequency of the ultrasonic transducer (f_0) in Eq. (6) is 12.5 MHz.

Using a similar process to that described in Section 3 and the contact deformation result, the equivalent FEM model of the roller-raceway contact is further meshed, as displayed in Fig. 7. The reference wave can be obtained by replacing the oil with air. The reflection coefficient, namely the simulated reflection coefficient, was calculated using Eq. (4).

4.2 Error evaluation of the ray model

For a comprehensive understanding of the coupling effects of loads and speeds, 30 combinations of conditions including five rotation speeds (100, 300, 500, 700, and 900 rpm) and six loads (100, 300, 600, 900, 1,200, and 1,500 N) were adopted. The reflection coefficients from both the simulations and calculations using the ray model were extracted for comparison. For differentiation, R_{sim} represents the reflection coefficient of the entire transducer (0.6 mm width) in the FEM simulation.

Based on Eq. (5) and the iterative solution algorithm, the reflection coefficient of the central oil-film thickness can be calculated using the ray model and is denoted as $R_{\text{ray}}(h_{\text{center}})$. As a reference, the reflection coefficient of the central oil-film thickness in the FEM model, denoted as $R_{\text{actual}}(h_{\text{center}})$, was calculated based on Eq. (1).

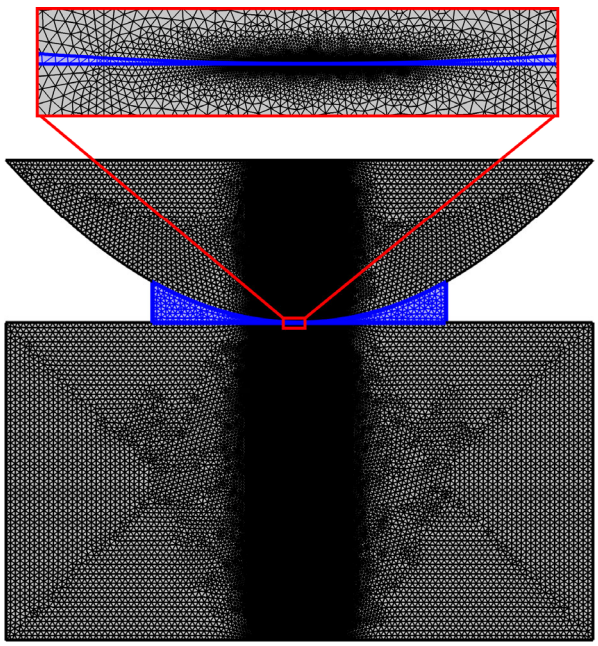

Fig. 7 Meshing results of equivalent model of roller-raceway contact.

The amplitudes of the reflection coefficients against the load are plotted in Fig. 8. The comparison is performed at the center frequency f_0.

As can be observed from Fig. 8, there are significant differences between $R_{\text{ray}}(h_{\text{center}})$ and ($R_{\text{actual}}(h_{\text{center}})$). With an increase in the load, the deviations decrease first and then increase. This can be analyzed from the contact variation in the loading. As the load increases, the contact zone becomes wider with less variation in the curves compared with the initiations. Therefore, fewer effects are introduced in the results of the ray model. However, in the same process, the changes in the distribution of the film bulk modulus become pronounced, as indicated in Fig. 6. These effects significantly influenced the simulation results. These characteristics explain the deviations of the ray model and simulation with increasing loading effects.

To further quantify the errors of the ray model, the oil-film thickness was calculated using the $R_{\text{ray}}(h_{\text{center}})$ under different operating conditions, as displayed in Fig. 8. Table 2 presents the relative error (%)* of the calculated central film thickness using the ray model to the central film thickness in the FEM model (i.e., the theoretical one) under different operating conditions.

It can be observed from Table 2 that the absolute relative error fluctuates between 0.04% and 213.76% under different conditions. Therefore, the error of the ray model is large and cannot be ignored, especially at low speeds.

4.3 Verification of error sources of the ray model

To verify that the errors of the ray model are caused by geometric scattering of wave propagation and nonuniform distribution of the oil bulk modulus, the equivalent models of the roller-raceway contact under different loads at a speed of 300 revolutions per minute (rpm) were used to verify the error sources.

Geometric scattering was studied first. The sound velocity and density of the oil film in both the contact and non-contact zones were set to 1,467 m/s and 850 kg/m^3, respectively, to ensure a uniform distribution of the bulk modulus of the oil film. Then, different loads in the range of 100–1,500 N were applied to obtain

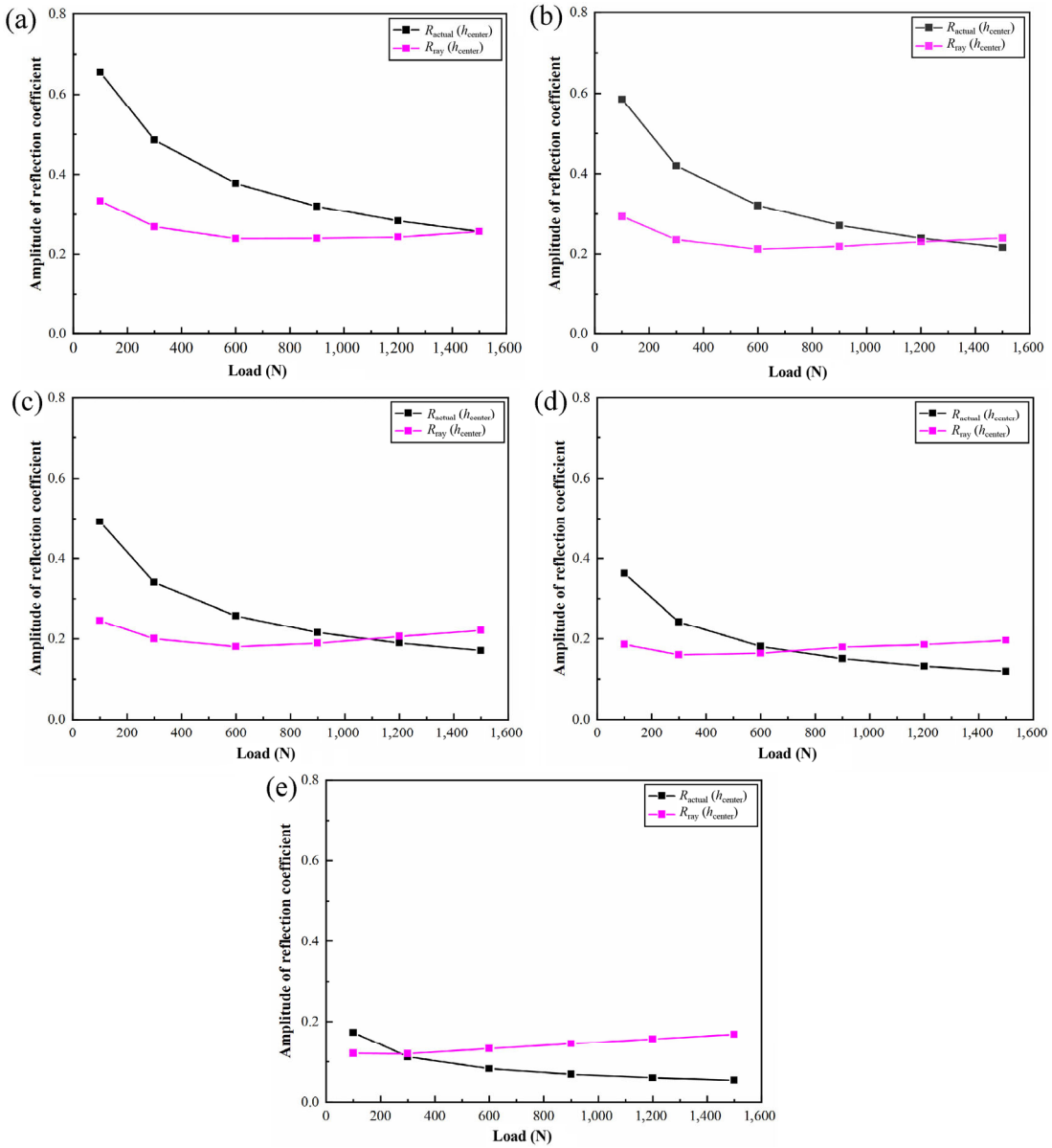

Fig. 8 Comparison of $R_{actual}(h_{center})$ and $R_{ray}(h_{center})$ under different operating conditions: (a) 900 rpm, (b) 700 rpm, (c) 500 rpm, (d) 300 rpm, and (e) 100 rpm.

Table 2 Relative error (%)* of calculated central film thickness using traditional ray model to central film thickness in FEM model (namely theoretical one) under different operating conditions.

Rotating speed (rpm)	Applied load (N)					
	100	300	600	900	1,200	1,500
	Contact width (μm)					
	50.64	87.70	113.24	151.92	175.42	196.14
100	30.42% (0.429)	−6.69% (0.388)	−59.99% (0.365)	−111.05% (0.351)	−161.57% (0.342)	−213.76% (0.335)
300	48.81% (0.954)	34.04% (0.863)	9.33% (0.811)	−19.09% (0.781)	40.58% (0.761)	−64.95% (0.746)
500	50.12% (1.383)	41.34% (1.252)	29.95% (1.175)	12.40% (1.133)	−8.55% (1.104)	17.417% (1.081)
700	49.77% (1.767)	43.83% (1.599)	34.25% (1.501)	19.20% (1.447)	2.98% (1.410)	−2.97% (1.381)
900	48.91% (2.121)	44.61% (1.919)	26.02% (1.802)	11.57% (1.737)	5.99% (1.692)	0.04% (1.658)

the corresponding deformed geometries. Figure 9 displays the reflection coefficients at the center frequency extracted from the simulation and ray model calculations. By comparison, clear deviations can be identified between the ray model and simulation results under the different loading conditions. The deviations decrease marginally with an increase in the load because the contact zone becomes wider with less variation in the curves compared with the initial values.

Following the above study of the geometric scattering effect, the influence of the nonuniform distribution of the bulk modulus of the oil film was then examined. The actual distribution of the bulk modulus in the contact and non-contact fields was adopted (Fig. 6). Because there is geometry scattering in the lubrication zone outside the contact zone, the ultrasonic reflection of this part cannot be considered. Therefore, to eliminate the influence of geometric scattering, the width of the transducer was set equal to that of the contact zone such that ultrasonic reflection only occurred in the contact zone. The reflection coefficients at the center frequency under different loads were extracted from the simulation and ray model calculation separately, the results of which are displayed in Fig. 10.

It can be observed both the i) nonuniformity degree of bulk modulus distribution in the contact zone, and ii) deviation between the ray model and simulation

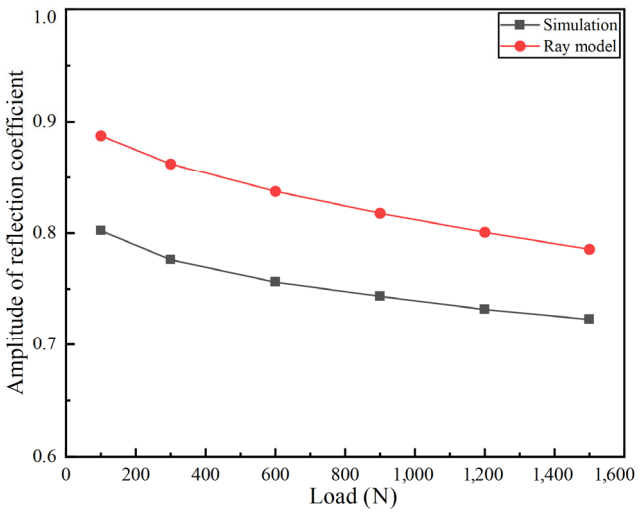

Fig. 9 Reflection coefficients of transducer obtained using simulation and ray model under different loads. Bulk modulus distribution is assumed to be uniform in simulation.

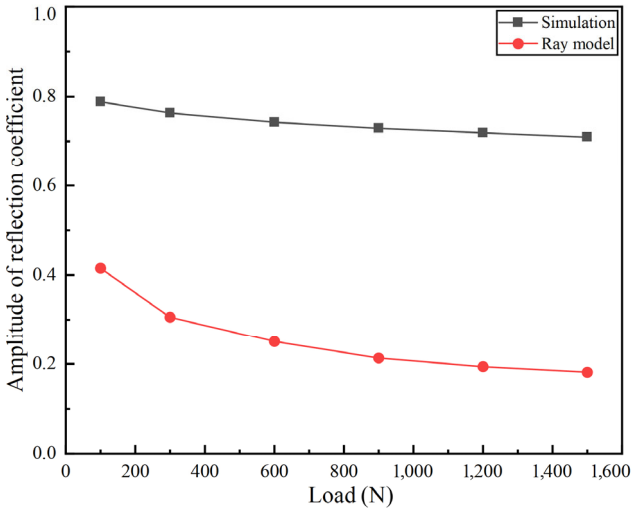

Fig. 10 Amplitudes of reflection coefficients of transducer obtained using simulation and ray model under different loads when bulk modulus distribution is nonuniform and width of transducer is set to that of contact zone under different loads.

increase as the load increases, from a minimum deviation of 0.17 at 100 N to a maximum deviation of 0.40 at 1,500 N.

With the above results, the two error sources and their mechanisms can be confirmed.

4.4 FEM-aided method for calculating the central oil-film thickness

From the above analysis, the simulated result is accurate, and hence, the simulation can be used to establish the relationship between the reflection coefficient of the central oil-film thickness and reflection coefficient received by the entire transducer. Here, coefficient R_k is introduced to establish the relationship between the two reflection coefficients.

$$R_k = \frac{R_{\text{sim}}}{R_{\text{sim}}(h_{\text{center}})} \tag{17}$$

Polynomial fitting was used to obtain R_k under different conditions, as indicated in Fig. 11. The coefficient of determination (R^2) and root mean squared error (RMSE) were 0.9990 and 0.1226, respectively.

With polynomial fitting, R_k can be denoted as a function of load W and speed U:

$$R_k = 6.743 + 0.01403W - 0.04131U - 3.321\times10^{-6}W^2 - 4.453\times10^{-5}WU + 0.0001206U^2 + 8.045\times10^{-9}W^2U$$

$$+5.567\times10^{-8}WU^2-1.505\times10^{-7}U^3-5.645\times10^{-12}W^2U^2$$
$$-2.313\times10^{-11}WU^3-1.505\times10^{-7}U^3-5.645\times10^{-12}W^2U^2$$
$$-2.313\times10^{-11}WU^3+6.647\times10^{-11}U^4 \tag{18}$$

In practical measurement, after the reflection coefficient of the entire transducer (denoted as R_{mea}) is obtained, when the load W and speed U are known, the practical reflection coefficient of the central oil-film thickness (denoted as $R_{\text{mea}}(h_{\text{center}})$) can be calculated by

$$R_{\text{mea}}\left(h_{\text{center}}\right)=\frac{R_{\text{mea}}}{R_k} \tag{19}$$

The central oil-film thickness can be calculated using Eq. (2).

It can be concluded that the FEM-aided method has two main improvements over the ray model. The first is the improved accuracy by compensating for the two types of errors. The second is the decreased computational cost without iterative calculations.

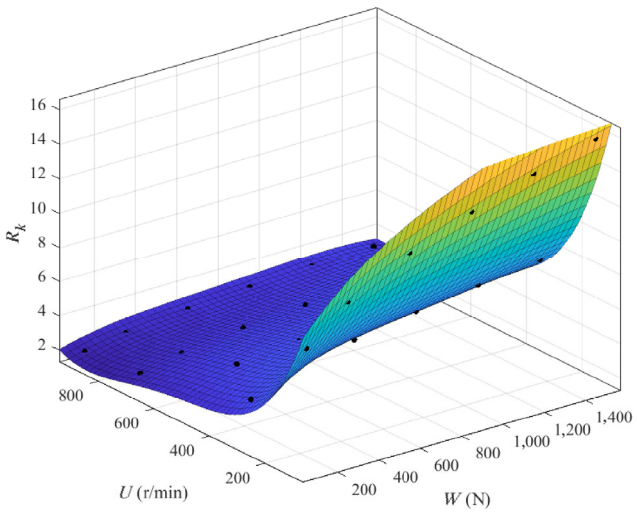

Fig. 11 Fitting result of R_k under different working conditions.

5 Experimental results for evaluation performance of the proposed FEM method

In this section, the proposed FEM-aided method is examined with a roller-raceway apparatus.

5.1 Experimental device

An experimental tester with a roller-raceway contact pair was prepared to imitate a rolling bearing in addition to a photograph of a roller and raceway, as displayed in Fig. 12.

The roller and raceway, from a real roller bearing, were adopted to serve as contact pairs and were driven separately by two motors. The speed of the roller was controlled by a 1.5 kW electric spindle with a range of 0–10,000 rpm and the speed of the inner ring was controlled by a 7.5 kW servomotor running at 0–1,000 rpm. This setup could facilitate the formation of oil films of different thicknesses by varying the relative speeds.

The oil between the raceway of the bearing and top roller was supplied by an oil supply system driven by a peristaltic pump. The lubricating oil was a synthetic turbine oil, Shell Turbo T68. The load was applied to the bearing by a lever through a pressure transducer.

Figure 13 displays the mounting of the ultrasonic transducer. The rectangular piezoelectric element was trimmed using a commercial circular ultrasonic transducer. The ultrasonic transducer was 6 mm in length, 0.6 mm in width, and 0.22 mm in thickness. It

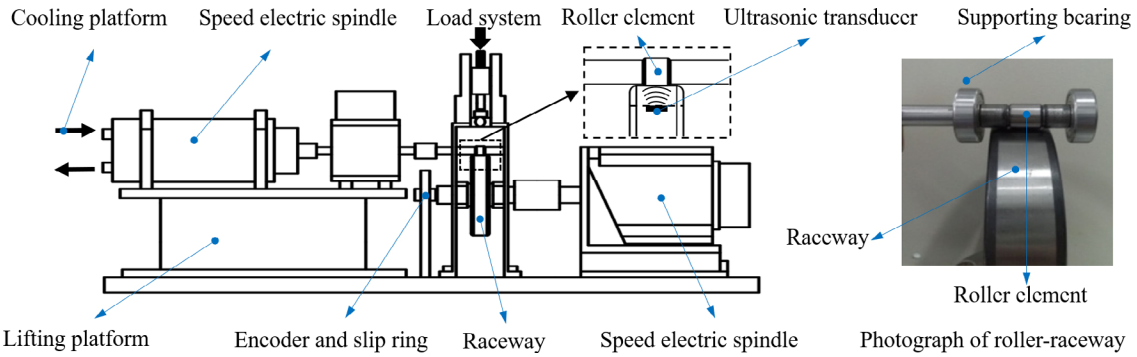

Fig. 12 Experimental setup with roller-raceway contact pair.

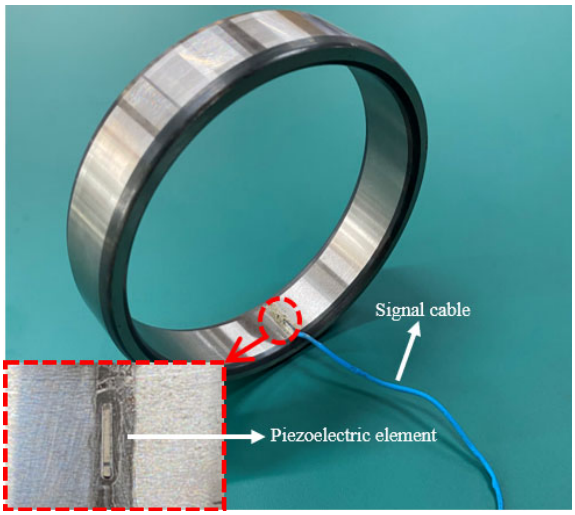

Fig. 13 Photograph of ultrasonic transducer on inner ring.

was glued to the inner surface of the ring sample using standard Mode600 adhesive. The shaft holding the ring sample was specially made hollow to lead the signal cable to a slip ring with carbon brushes. With this, the measured signal could be introduced from the rotating part into a computer-based measurement system. The encoder was also equipped to synchronously locate the contact in the continuous signal. The number of encodings, N_{encoder}, determines the precision of the measurement in the circumferential direction of the ring. Therefore, it was set to 1,000.

The FMS-100 supplied by Tribosonics Ltd., Co., was adopted as the ultrasonic measurement device to both send and receive the pulse simultaneously. The pulse repetition rate, denoted as f_{r}, was 20 kHz, and the hardware was configured in the pulse/receive mode; the same cable and transducer were used.

In the case of a low inner ring speed, the measurement speed was considerably faster than the encoder rotation speed, and several measurements were marked in the same position. The number of measurements at each observation zone divided by the encoder number is denoted as N.

$$N = \frac{f_{\text{r}} \cdot 60}{N_{\text{encoder}} \cdot n_{\text{speed}}} = \frac{1,200}{n_{\text{speed}}} \tag{20}$$

where n_{speed} is the rotation speed (rpm).

To ensure accuracy, N should be greater than one in each observation zone. The final result for each observation zone was the average of multiple measurements in the zone.

In the tests, a wide range of loads and speeds were adopted to produce oil films of different thicknesses. Specifically, the loads were 500, 1,000, 1,500, and 2,000 N and the speed was set to 500, 700, and 900 rpm. The test included 18 combination conditions. The operating range of the experiment was the same as that for the simulation analysis. The relevant acoustic properties of the oil and bearing steel were measured and are provided in Table 3.

Table 3 Properties of different materials in three-layered structures.

Material	Density ($\text{kg}\cdot\text{m}^{-3}$)	Acoustic speed ($\text{m}\cdot\text{s}^{-1}$)	Bulk modulus, B (GPa)
Oil (0.1)	850	1,467	1.83
Oil (0.65)	1,007	2,854	8.20
Oil (0.97)	1,037	3,282	11.17
Bearing steel	7,810	5,818	200

5.2 Experimental results

Ultrasonic pulses with duration of 0.8 μs were captured and compiled in real-time, forming raw ultrasonic data streams, as indicated in Fig. 14. From the encoded data, it can be observed that the reduction in signal amplitude corresponded to the transducer passing through the contact zone. The amplitude attenuation of echo waves is mainly due to the transmission of sonic waves into the roller, which has lower acoustic impedance than air.

For each pulse from the raw ultrasonic data, the reflected echo was transformed into a frequency domain and the amplitude at the center frequency was extracted. A dip appears when the piezoelectric element passes below the roller, as indicated in Fig. 15.

Different phenomena can be observed in Fig. 15. First, there are numerous vibration phenomena around the dips. Similar results were reported in Refs. [18, 34, 35]. These could be caused by measurement uncertainties such as electronic noise, surface roughness, and contact vibration.

Secondly, unexpected values of the reflection coefficients greater than one can be observed; similar abnormity was reported in Refs. [13, 35]. This phenomenon can be explained by the superposition

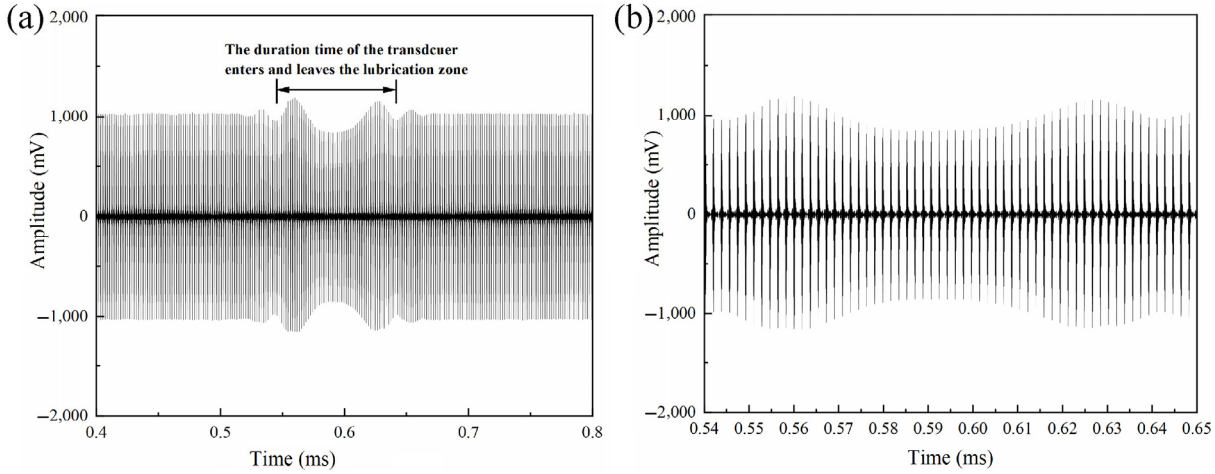

Fig. 14 (a) Raw ultrasonic data for period of time and (b) an enlarged view with commence and end time indicating moment transducer enters and leaves lubrication zone, respectively: (a) raw ultrasonic data and (b) enlarged view of contact zone.

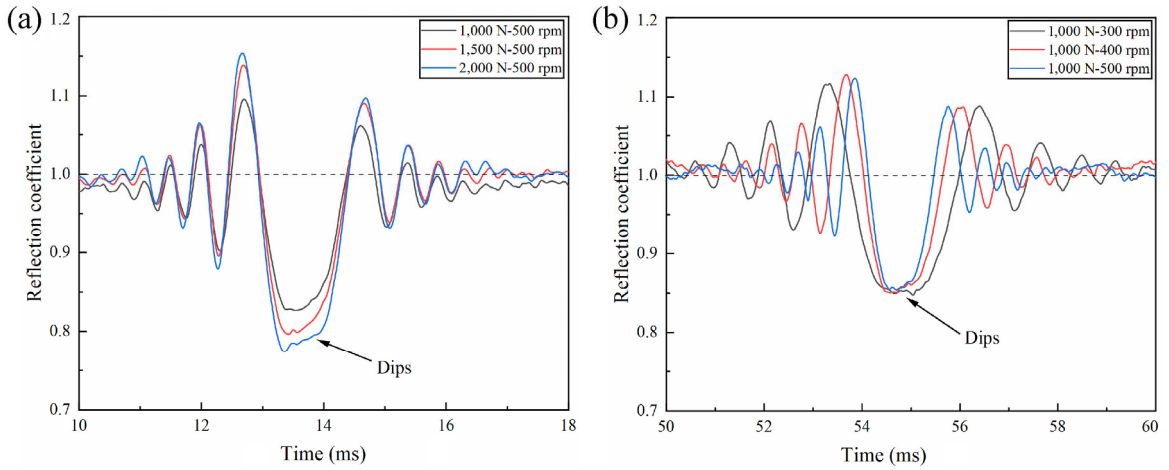

Fig. 15 Reflection coefficient recorded for (a) different loads at speed of 500 rpm and (b) different speeds at load of 1,000 N.

principle of waves [13]. When the oil-film thickness increases beyond the effective scope of the spring model, the pulse echoes are more likely to be scattered by the curvature surface of the roller and only partially received by the ultrasonic transducer, where the waves are summed as in the vector space, and the overall magnitude can be either greater or less than that of the incident pulse wave, according to Ref. [13]. Conversely, this phenomenon of "greater than one" does not violate the law of energy conservation as the total wave energy received by the transducer which is calculated using the sum of the energy of each echo wave, rather than using the energy of the overall wave vector. More information regarding the calculation of the energy of sound waves can be found in Ref. [36].

Thirdly, the shape of the dip is asymmetrical, which makes it difficult to identify the minimum oil- film thickness. In the current work, the middlemost point of the dip with a reflection coefficient of less than one is adopted for the symmetrical assumption of the contact. Consequently, the measured reflection coefficient (R_{m}) can be calculated using Eq. (4).

With the measured reflection coefficient (R_{mea}), the reflection coefficient of the central oil-film thickness ($R_{\mathrm{mea}}(h_{\mathrm{center}})$) can be calculated using Eqs. (18) and (19), and the central oil film thickness (h_{center}) can be calculated using Eq. (2). For comparison, the oil-film thicknesses calculated by the FEM-aided method, ray model [20], and spring model [16] are also presented. Here, the reference spring model uses the overall reflection coefficient of the transducer (R_{mea}).

Figure 16 displays the results under different load

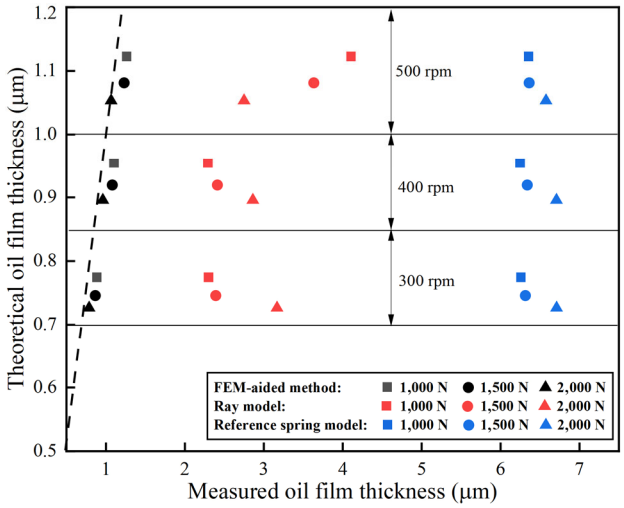

Fig. 16 Comparison of experimentally measured oil film thickness with EHL theoretical solution (Eq. (7)) for range of bearing load W and speed U. Dashed line represents EHL theoretical solution (Eq. (7)).

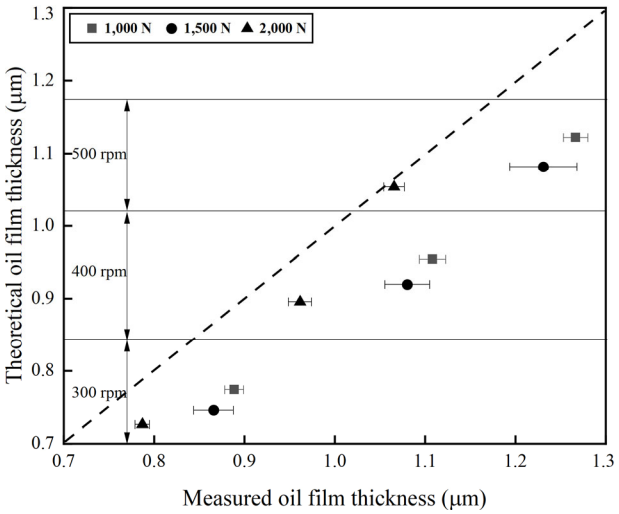

Fig. 17 Result of oil-film thickness of 20 measurements using FEM-aided method. Dashed line represents EHL theoretical solution (Eq. (7)).

and speed conditions. It can be observed that the reference spring model presents the most significant deviations from the theoretical EHL solution (Eq. (7)). Compared to the ray model, the proposed FEM-aided method can provide a decent improvement in terms of measurement accuracy.

5.3 Error source discussion

The method of integrating ultrasound simulation and EHL theory improved the measurement accuracy of the ray model. Figure 17 displays the results of the oil-film thickness of 20 measurements obtained using the FEM-aided method.

To examine the reliability of the FEM-aided method, multiple measurements were performed. Figure 17 displays the results of the 20 tests. Under the same test conditions, the theoretical value is calculated with the classical EHL model, and the measured value is obtained with the FEM-aided method as described above. The deviation of the measured value from the theoretical value is defined as the error. The error sources are the focus of the following discussion.

It can be observed from Fig. 17 that errors exist between the two methods. The error sources can be discussed based on these aspects:

1) The rectangular piezoelectric element is simplified as a line source in the finite element model to reduce computational cost. Therefore, there is an inherent simulation error between the three-dimensional and two-dimensional finite element models.

2) There is an inherent error between the theoretical EHL theory and actual test. The bulk modulus distribution is based on an empirical equation, which is not accurate. Furthermore, the viscosity of the oil was assumed to be constant during the test. However, the temperature of the oil increased when the rig was operating at a higher speed. Therefore, the oil film would be thinner owing to the decrease in viscosity. This explains why the error of the measured value to the theoretical increased with speed.

3) It can be observed that the measured oil-film thickness was always greater than the theoretical calculation values. This could have been caused by a certain deviation of the axis line of the roller and raceway during assembly; conversely, the mixed lubrication of the roller and raceway causes surface wear during the operation, which could also cause an error in the final result (to a certain degree).

4) In our simulations and theoretical calculations, the surface roughness was not considered for simplicity; however, neglecting the surface roughness could result in an error in both the measured film thickness and theoretical value [37].

5) The effect of rheology was not considered in this study. Rheology can influence the pressure distribution in the contact zone and alter the distribution of the bulk modulus [30]. Based on Eq. (2), the accuracy of

the film thickness calculation is influenced.

6) The complex curvature of the deformed surfaces of the roller and raceway could not be completely and accurately established; in the simulation process, the elastic contact deformation between the roller and raceway was equivalent to the elastic contact deformation between an equivalent cylinder and a rigid plane. However, the actual deformation is considerably more complex and typically requires a sophisticated numerical solution; therefore, the deformation discrepancy from the assumptions made in the present work could introduce film-thickness measurement errors. These issues will be explored further in future research.

7) The large size of the sensor compared with the contact zone could cause a large deviation from the central film thickness with respect to the spatial resolution. The quantitative influence on this relationship should be further analyzed.

6 Conclusions

In this work, an FEM-aided method was proposed to improve the spatial resolution of the thickness measurement of the oil film in a roller bearing. First, a two-dimensional finite element model was established to simulate ultrasonic wave propagation in a parallel steel–oil–steel interface. By comparing the reflection coefficient obtained by the theoretical calculation with that obtained by simulation, the effectiveness of the FEM method was verified. Then, the FEM method was applied to a roller–raceway contact; the simulation results demonstrated that the errors of the ray model derived from geometric scattering and the distribution nonuniformity of the oil bulk modulus. With the FEM employed again in a roller–raceway under EHL, an accurate relationship between the objective variable of the central oil-film thickness and reflection coefficient (directly measured by the embedded ultrasonic transducer) was established. Experimental results with varied loads and speeds demonstrated that the proposed FEM-aided method enabled highly accurate measurements of oil-film thickness (as compared with the conventional ray and spring models) by demonstrating acceptable agreement with the theoretical values.

In future research, it is necessary to establish an actual and accurate roller–raceway contact model and consider the influence of the roughness and rheological properties of lubricant oil on the measurement results. The effect of surface roughness and rheology could have also caused errors in the proposed method. Their influence will be evaluated in a future study. Furthermore, the influence of the transducer width on the simulation measurement results must be further analyzed. In addition, a study of the optimal element size is required to balance the measurement accuracy and computational cost.

Acknowledgements

The authors appreciate the financial support from the National Natural Science Foundation of China (Nos. 51675403 and 51975455) and the Fundamental Research Funds for the Central Universities (No. xzy022020005).

References

[1] Stachowiak G W, Batchelor A W. *Engineering Tribology*. Amsterdam (USA): Elsevier, 2006.

[2] Wen S, Huang P. *Principles of Tribology*. Beijing (China): Tsinghua University, 2011.

[3] Grubin A N. Fundamentals of the hydrodynamic theory of lubrication of heavily loaded cylindrical surfaces. In

Proceedings of the Symposium on Investigation of the Contact of Machine Components, Moscow, Russia, 1949: 115–166.

[4] Dowson D, Higginson G R. *Elasto-Hydrodynamic Lubrication*. Amsterdam (the Netherlands): Elsevier, 1977: 65–77.

[5] El-Sisi S I, Shawki G S A. Measurement of oil-film thickness between disks by electrical conductivity. *ASME J Basic Eng* **82**:12–8 (1960)

[6] Astridge D G, Longfield M D. Paper 11: Capacitance measurements and oil film thickness in a large-radius disc and ring machine. *Proc Inst Mech Eng Conf Proc* **182**(14): 89–96 (1967)

[7] Vlădescu S C, Medina S, Olver A V, Pegg I G, Reddyhoff T. Lubricant film thickness and friction force measurements in a laser surface textured reciprocating line contact simulating the piston ring-liner pairing. *Tribol Int* **98**: 317–329 (2016)

[8] Jablonka K, Glovnea R, Bongaerts J. Quantitative measurements of film thickness in a radially loaded deep-groove ball bearing. *Tribol Int* **119**: 239–249 (2018)

[9] Zhang Y G, Wang W Z, Zhang S G, Zhao Z Q. Optical analysis of ball-on-ring mode test rig for oil film thickness measurement. *Friction* **4**(4): 324–334 (2016)

[10] Ma L R, Luo J B. Thin film lubrication in the past 20 years. *Friction* **4**(4): 280–302 (2016)

[11] Dwyer-Joyce R S, Harper P, Drinkwater B W. A method for the measurement of hydrodynamic oil films using ultrasonic reflection. *Tribol Lett* **17**(2): 337–348 (2004)

[12] Dou P, Wu T H, Luo Z P. Wide range measurement of lubricant film thickness based on ultrasonic reflection coefficient phase spectrum. *J Tribol* **141**(3): 031702 (2019)

[13] Dou P, Wu T H, Luo Z P, Peng Z X, Sarkodie-Gyan T. The application of the principle of wave superposition in ultrasonic measurement of lubricant film thickness. *Measurement* **137**: 312–322 (2019)

[14] Yu M, Shen L, Mutasa T, Dou P, Wu T H, Reddyhoff T. Exact analytical solution to ultrasonic interfacial reflection enabling optimal oil film thickness measurement. *Tribol Int* **151**: 106522 (2020)

[15] Dou P, Wu T H, Peng Z X. A time-domain ultrasonic approach for oil film thickness measurement with improved resolution and range. *Meas Sci Technol* **31**(7): 075006 (2020)

[16] Zhang J, Drinkwater B W, Dwyer-Joyce R S. Acoustic measurement of lubricant-film thickness distribution in ball bearings. *J Acoust Soc Am* **119**(2): 863 (2006)

[17] Dwyer-Joyce R S, Reddyhoff T, Drinkwater B W. Operating limits for acoustic measurement of rolling bearing oil film thickness. *Tribol Trans* **47**(3): 366–375 (2004)

[18] Drinkwater B W, Zhang J, Kirk K J, Elgoyhen J, Dwyer-Joyce R S. Ultrasonic measurement of rolling bearing lubrication using piezoelectric thin films. *J Tribol* **131**(1): 011502 (2009)

[19] Mills R, Vail J R, Dwyer-Joyce R. Ultrasound for the non-invasive measurement of internal combustion engine piston ring oil films. In *Proceedings of the Institution of Mechanical Engineers*. *Part J: J Eng Tribol* **229**(2): 207–215 (2015)

[20] Zhang K, Meng Q F, Chen W, Li J N, Harper P. Ultrasonic measurement of oil film thickness between the roller and the inner raceway in a roller bearing. *Ind Lubr Tribol* **67**(6): 531–537 (2015)

[21] Li M, Liu H, Xu C, Jing M Q, Xin W H. Ultrasonic measurement of cylindrical roller bearing lubrication using high pulse repletion rates. *J Tribol* **137**(4): 042202 (2015)

[22] Li M, Jing M Q, Chen Z F, Liu H. An improved ultrasonic method for lubricant-film thickness measurement in cylindrical roller bearings under light radial load. *Tribol Int* **78**: 35–40 (2014)

[23] Hunter A, Dwyer-Joyce R, Harper P. Calibration and validation of ultrasonic reflection methods for thin-film measurement in tribology. *Meas Sci Technol* **23**(10): 105605 (2012)

[24] Dwyer-Joyce R S, Drinkwater B W, Donohoe C J. The measurement of lubricant–film thickness using ultrasound. Proc R Soc Math Phys Eng Sci 459(2032): 957–976 (2003)

[25] Jensen J A, Svendsen N B. Calculation of pressure fields from arbitrarily shaped, apodized, and excited ultrasound transducers. *IEEE Trans* Ultrason Ferroelectr Freq Control 39(2): 262–267 (1992)

[26] Information on https://doc.comsol.com/5.4/doc/com.comsol.help.sme/StructuralMechanicsModuleUsersGuide.pdf.

[27] Information on https://doc.comsol.com/5.4/doc/com.comsol.help.aco/AcousticsModuleUsersGuide.pdf.

[28] Liu J, Xu G C, Ren L, Qian Z H, Ren L Q. Simulation analysis of ultrasonic detection for resistance spot welding based on COMSOL Multiphysics. *Int J Adv Manuf Technol* **93**(5–8): 2089–2096 (2017)

[29] Demirli R, Saniie J. Model-based estimation of ultrasonic echoes. Part I: Analysis and algorithms. *IEEE Trans Ultrason Ferroelectr Freq Control* **48**(3): 787–802 (2001)

[30] Bair S. Conclusion. *High Pressure Rheology for Quantitative Elastohydrodynamics*. Amsterdam (the Netherlands): Elsevier, 2019.

[31] Dwyer-Joyce R S, Reddyhoff T, Zhu J. Ultrasonic measurement for film thickness and solid contact in elastohydrodynamic lubrication. *J Tribol* **133**(3): 031501 (2011)

[32] Fakhreddine Y A, Zoller P. The equation of state of a polydimethylsiloxane fluid. *J Appl Polym Sci* **41**(5–6): 1087–1093 (1990)

[33] Li M, Liu H, Xu C, Jing M Q, Dong G H. Ultrasonic measurement of cylindrical roller-bearing lubricant film distribution with two juxtaposed transducers. *Tribol Trans* **60**(1): 79–86 (2017)

[34] Wan Ibrahim M K, Gasni D, Dwyer-Joyce R S. Profiling a ball bearing oil film with ultrasonic reflection. *Tribol Trans* **55**(4): 409–421 (2012)

[35] Nicholas G, Howard T, Long H, Wheals J, Dwyer-Joyce R S. Measurement of roller load, load variation, and lubrication in a wind turbine gearbox high speed shaft bearing in the field. *Tribol Int* **148**: 106322 (2020)

[36] Kinsler L E, Frey A R, Coppens A B, Sanders J V. *Fundamentals of Acoustics*. 4th edn. New Jersey (USA): John Wiley & Sons Inc, 2000.

[37] Masjedi M, Khonsari M M. Film thickness and asperity load formulas for line-contact elastohydrodynamic lubrication with provision for surface roughness. *J Tribol* **134**(1): 011503 (2012)

Pan DOU. He received his B.S. degree in mechanical design manufacture and automation from Taiyuan University of Technology, Taiyuan, China, in 2016. He is currently studying his Ph.D. degree in mechanical engineering from Xi'an Jiaotong University, Xi'an, China. His ongoing research focuses on the ultrasonic measurement of oil film thickness and wear.

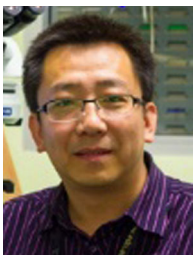

Tonghai WU. He received his Ph.D. degree in mechanical engineering from Xi'an Jiaotong University, Xi'an, China, in 2006. He is currently a professor at the School of Mechanical Engineering, Xi'an Jiaotong University. From 2013 to 2014, he was a visiting scholar with the University of New South Wales, Australia. His current research interests include machinery diagnosis, and prognosis, machine vision on wear particle, and surface analysis.

Zhaopeng LUO. He received his M.S. degree from Xi'an Jiaotong University, Xi'an, China, in 2020. He is now working as a civil servant in Chengdu. His research interest is the ultrasonic measurement of oil film thickness.

Peiping YANG. He received his M.S. degree from Xi'an Jiaotong University, Xi'an, China, in 2009. He is now working as a senior engineer in Dongfang Electrical Machinery Co., Ltd., Sichuan, China. His research interests include lubrication of bearings, tribology, condition monitoring, and fault diagnosis.

Zhongxiao PENG. She received her Ph.D. degree in mechanical engineering from the University of Western Australia, Australia, in 2000. She is currently a professor in the School of Mechanical and Manufacturing Engineering, University of New South Wales (UNSW Sydney, Australia). Her current research interests include wear analysis of mechanical and bio-engineering components and systems, 3D imaging and image characterisation of worn surfaces and wear debris, machine condition monitoring using wear debris analysis, vibration, and artificial intelligence technology.

Min YU. He received his B.Eng. degree in mechanical engineering from Xi'an Jiaotong University, Xi'an, China, in 2011, M.Sc. degree in mechatronic control engineering from Zhejiang University, Hangzhou, China, in 2014, and his Ph.D. degree in control engineering at Imperial College London, in 2018. He is currently a research associate in the Department of Mechanical Engineering, Imperial College London. His research interests include mechatronics and robotics, dynamics and control, non-destructive sensing, and lubricant testing. He has specialized in developing embedded platforms and prototypes to validate newly proposed concepts and techniques, as in combination with analytical models and numerical simulations.

Tom REDDYHOFF. He received his M.Eng. and Ph.D. degrees in mechanical engineering from the University of Sheffield in 2003 and 2006, respectively. He is currently a Reader in the Department of Mechanical Engineering and a member of the Tribology Group. He is a mechanical engineer, but the scope of his research has broadened to include the chemistry and physics of surfaces. He has specialized in developing a range of experimental methods, which he uses in combination with numerical modelling to analyze sliding interfaces. He holds a five-year EPSRC Career Acceleration Fellowship. He has received the Tribology Trust Bronze Medal, a Tiaho Young Tribologist Award, and two best paper awards.